Preparation of S-doped $CuCoO_2$ nanosheets with more oxygen defects for efficient oxygen evolution reaction

Chao Jiang, [a] Jilin Bai, [a] Qingyang Shen, [a] Xin Ku, [a] Wei Liao, [a, b] and Dehua Xiong*, [a]

a. State Key Laboratory of Silicate Materials for Architectures, Wuhan University of Technology, Wuhan 430070, P. R. China.

b. Songshan Lake Materials Laboratory, Dongguan, 523808, P. R. China.

* Corresponding author.

E-mail addresses: xiongdehua2010@gmail.com (Dehua Xiong)

Experimental details

Materials synthesis

All chemicals in the experiment were of analytical grade without further purification. Cu-BTC and $CuCoO_2$ were prepared according to our previous work.[1]

Cu-BTC synthesis: Firstly, 2.6093 g $Cu(NO_3)_2 \cdot 3H_2O$, 1.2600 g H_3BTC and 9 mL isopropyl alcohol (IPA) were dissolved in 27 mL deionized (DI) water and 36 mL absolute ethanol (ET), and magnetically stirring for 30 minutes. Secondly, the solution was transferred into a 100 mL Teflon lined autoclave and kept at 120 °C for hydrothermal reaction for 12 h. Afterwards, the resulting blue precipitate was washed three times with ET to remove any by-product impurities. Finally, the Cu-BTC was dried at 70 °C for 5 h for further use.

S-doped $CuCoO_2$ synthesis: Firstly, 1.50 g Cu-BTC, 1.60 g (5.5mmol) $Co(NO_3)_2 \cdot 6H_2O$, S (0, 0.11, 0.33 and 0.55 mmol) and 1.40 g NaOH were dissolved in DI water and ET, and magnetically stirring for 30 minutes. Secondly, the 3.3342 g PVP (K23-27) was added to the above solution and stirred for 1 h. Afterwards, the solution was transferred into a 100 mL Teflon lined autoclave and kept at 140 °C for hydrothermal reaction for 24 h. Finally, the obtained precipitate was washed several times with ammonia, DI water, and ET, and then dried at 70 °C for 5 h for further characterization.

Structural characterization

The crystal phase of samples was characterized by the X-ray diffraction (XRD, D8 Advance, Bruker, Germany). The radiation source is Cu Kα radiation (wavelength λ = 1.54184 Å), run with a typical operating voltage of 40 kV at 40 mA, and the XRD patterns were obtained in steps of 0.02° in the 2θ range of 10°~80° at a scan rate of 10 °/min. The morphology, microstructure, and chemical composition of the samples were examined by field-emission scanning electron microscopy (FESEM, Sigma 300, Zeiss, Germany) and transmission electron microscopy (TEM, JEM-2100 operating at 200 keV, JEOL, Japan) equipped with energy-dispersive X-ray spectroscopy (EDS, X-Max, Oxford, Britain). The as-prepared $CuCoO_2$ based powder was adhered on carbon conductive tape for SEM observation. Regarding for TEM measurement, the $CuCoO_2$ based powder was dispersed in ethanol and loaded on Mo grids for characterization. The surface chemical states of the samples were analyzed by X-ray photoelectron spectroscopy (XPS, Escalab 250Xi, Thermo Fisher Scientific, USA). The X-ray source uses Al target as the excitation source with high-energy electrons. The deconvolution

analysis of XPS spectrum was processed using the Avantage software. The structure of samples was investigated by Raman (LabRAM Odyssey, HORIBA Scientific, France) and Fourier Transform Infrared (Nicolet 6700, Thermo Fisher Scientific, USA), and their resolutions are 0.65 cm^{-1}, 0.019 cm^{-1}, respectively. The Brunauer-Emmett-Teller (BET) specific surface areas and porosity parameters of the $CuCoO_2$ based powder samples (~ 0.50 g) were taken by N_2 adsorption-desorption isothermetry (TriStar II 3020, Micromeritics, USA) at liquid N_2 temperature. The optical absorption curve of samples in 200-2500 nm range was measured by UV-visible near-infrared spectrophotometer (UV-Vis-NIR, Lambda 750 S, PerkinElmer, USA) with a step size of 5 nm. and the band gap value was calculated.

Electrode preparation and electrochemical measurement

Firstly, 15 mg $CuCoO_2$ was dissolved in 500 μL DI water, 480 μL IPA and 20 μL Nafion (5 wt%, Sigma) to make a suspension, then 20 μL of the suspension solution was placed on Ni foam (1 cm×1 cm), and finally the working electrode was prepared by drying at 150 °C for 10 min. The working electrodes prepared with CCO and CCOS-x were named Ni@CCO and Ni@CCOS-x, respectively.

The OER performance was evaluated by cyclic voltammetry (CV) and electrochemical impedance spectroscopy (EIS) in a three-electrode configuration in 1.0 M KOH (pH = 13.5) using a CS2350H electrochemical workstation (Wuhan Corrtest Instruments Corp, China). A platinum wire and a saturated calomel electrode (SCE) were used as the counter and reference electrodes, respectively. Cyclic voltametric (CV) scans were recorded between 1.05 and 1.80 V vs. reversible hydrogen electrode (RHE) at a scan rate of 2 $mV \cdot s^{-1}$. The electrochemical double-layer capacitance (C_{dl}) can be extracted through CV scans recorded at different rates (from 20 to 100 $mV \cdot s^{-1}$) in the non-faradaic potential window of -0.05-0.05 V vs. SCE. The EIS measurements were performed in the frequency range of 0.1 MHz – 0.1 Hz under a constant potential of 1.63 V vs. RHE. Under the constant current density of 10 mA cm^{-2}, the stability of the sample was tested for 18 hours.

All current density values are normalized with respect to the geometrical surface area of the working electrode. All CV curves presented in this work are iR-corrected (85%). The correction was done according to the following equation:

$$E_c = E_m - iR_s \quad \text{(S1)}$$

where E_c is the iR-corrected potential, Em experimentally measured potential, and R_s the equivalent series resistance extracted from the electrochemical impedance spectroscopy

measurements. Unless otherwise specified, all potentials are reported vs. RHE by converting the potentials measured vs. SCE according to the following formula:

$$E\ (RHE) = E\ (SCE) + 0.241 + 0.059\ pH \quad (S2)$$

ECSA can be calculated by the equation:

$$ECSA = (C_{dl}/C_s) \quad (S3)$$

C_{dl} is the double-layer capacitances value. C_s is the specific capacitance (typically 0.04 mF cm^{-2}).

Supplementary tables:

Table S1. Detailed reaction conditions for synthesizing delafossite $CuCoO_2$ nanocrystals.

Sample	Cu-BTC (g)	$Co(NO_3)_2 \cdot 6H_2O$ (mmol)	S (mmol)	NaOH (g)	PVP (g)	Solvent (mL)	Temp. (°C)	Time (h)
CCO	1.5	5.5	0	1.40	3.3342	50 ET: 20 DI	140	24
CCOS-1			0.11					
CCOS-3			0.33					
CCOS-5			0.55					

Table S2. The OER performance of these electrodes in this work compared with other oxide catalysts.

Catalyst	Electrolyte	η_{10} (mV)	Tafel slope (mV dec^{-2})	(year)[Ref.]
Ni@CCOS-3	1.0 M KOH	**375.5**	**83.4**	**This work**
Fe doped $CuCoO_2$		369	69	(2023)[1]
PEG assisted $CuCoO_2$		378	85	(2023)[2]
CNTs supported $CuCoO_2$		343	65	(2024)[3]
$CuGaO_2$		400	61	(2022)[4]
$NiFe_2O_4$		366	84.2	(2023)[5]
$MgCo_2O_4$		470	95	(2023)[6]
$LaNi_{0.75}$-$Fe_{0.25}O_3$		292	58.8	(2023)[7]
$La_{0.5}Sr_{0.6}Fe_{0.8}Cu_{0.15}Nb_{0.05}O_3$		381	120	(2024)[8]
$CoMn_2O_4$-S_2		350	88	(2021)[9]
S-MnO_x/Mn/CP		435	89.97	(2022)[10]
CuO/CuS		270	67	(2023)[11]
CuO/Mn_3O_4		293 (η_{20})	106.2	(2023)[12]
$CuCo_2O_4$ (Nanoflower)		288	64.2	(2020)[13]
CuCoO (Nanowire)		270	68	(2016)[14]
N, Fe co-doped CoO/Co_3N		304	59.8	(2021)[15]

Table S3. BET specific surface area, pore volume and pore diameter of CCO and CCOS-x (x=1, 1, 3 and 5).

Sample	BET specific surface area ($m^2\ g^{-1}$)	pore volume ($cm^3\ g^{-1}$)	pore diameter (nm)
CCO	3.64	0.01347	33.4334
CCOS-1	9.88	0.02293	21.4587
CCOS-3	12.51	0.03371	10.8345
CCOS-5	9.99	0.02223	14.3714

Supplementary figures:

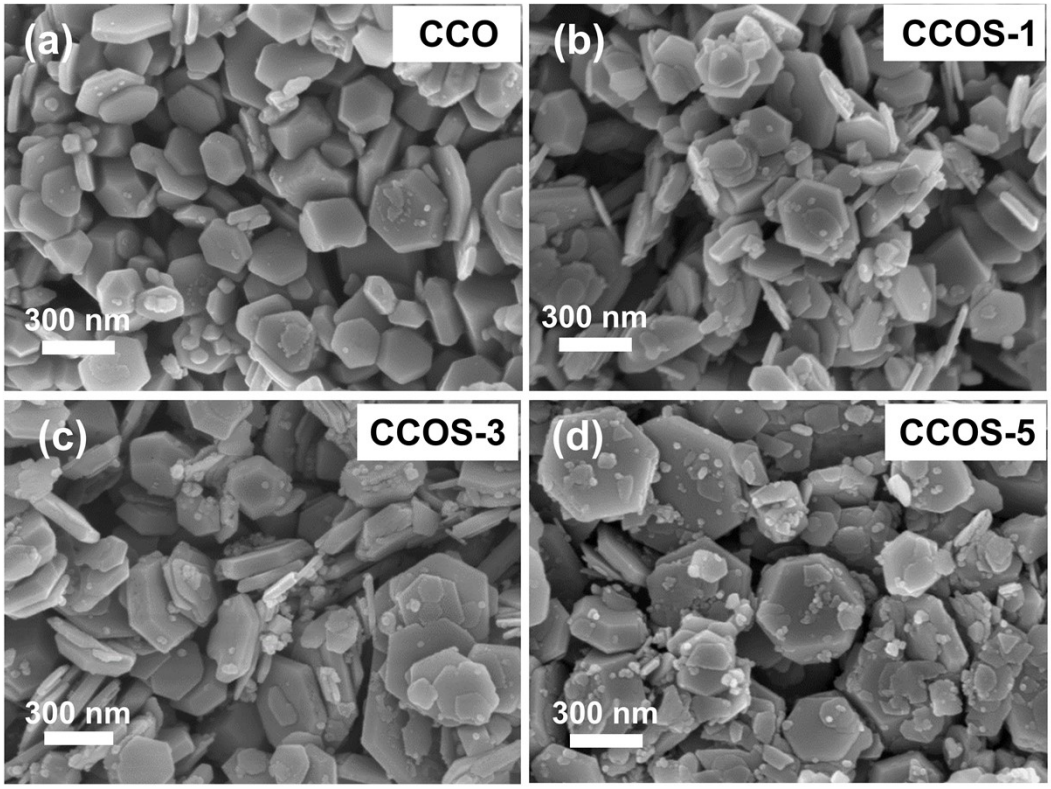

Fig. S1 (a-d) SEM images of CCO and CCOS-x (x=1, 3 and 5) samples.

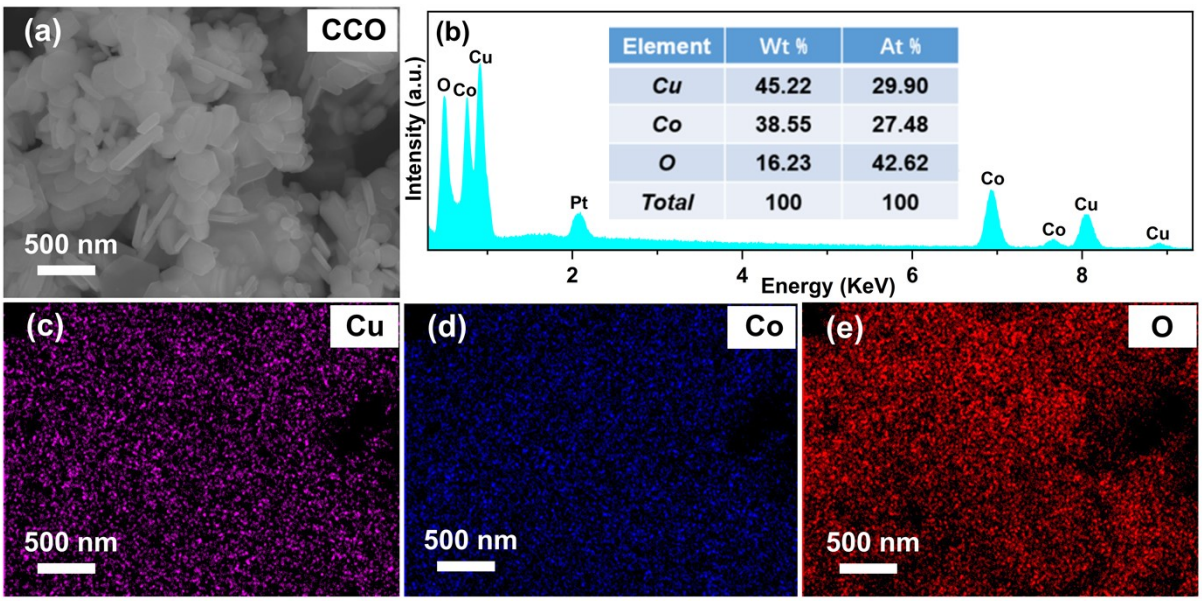

Fig. S2 (a) SEM image, (b) EDS spectrum and (c-e) elemental maps of CCO.

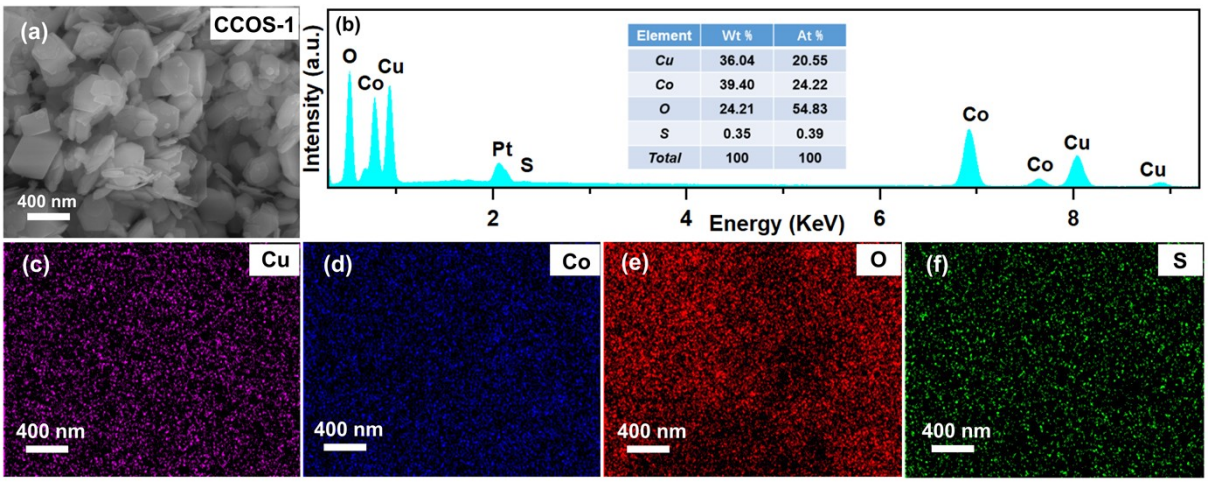

Fig. S3 (a) SEM image, (b) EDS spectrum and (c-f) elemental maps of CCOS-1.

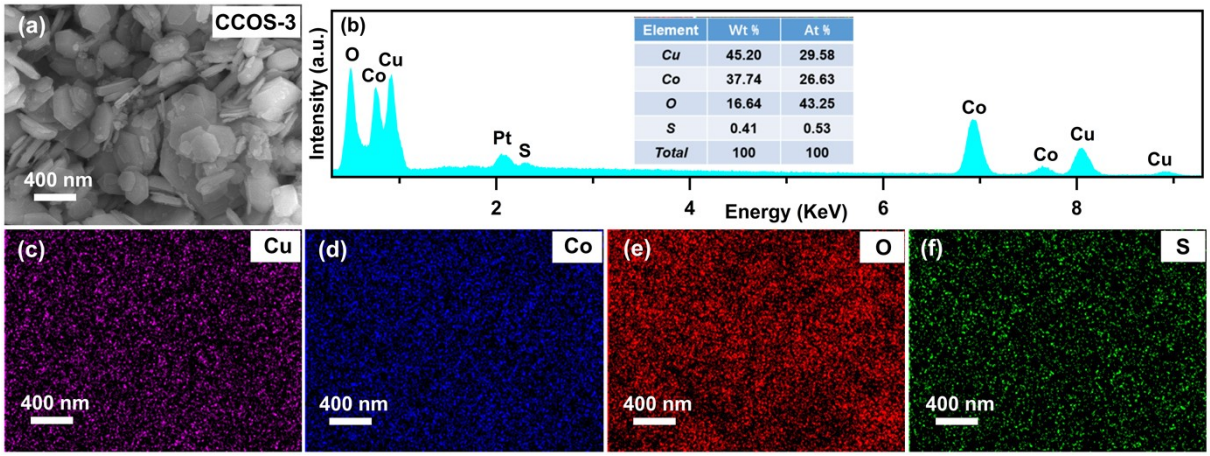

Fig. S4 (a) SEM image, (b) EDS spectrum and (c-f) elemental maps of CCOS-3.

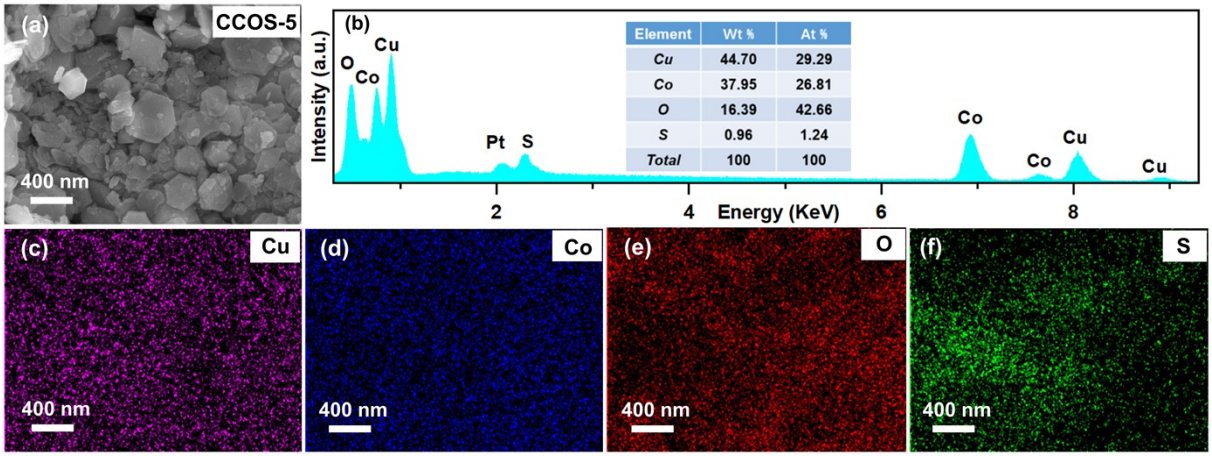

Fig. S5 (a) SEM image, (b) EDS spectrum and (c-f) elemental maps of CCOS-5.

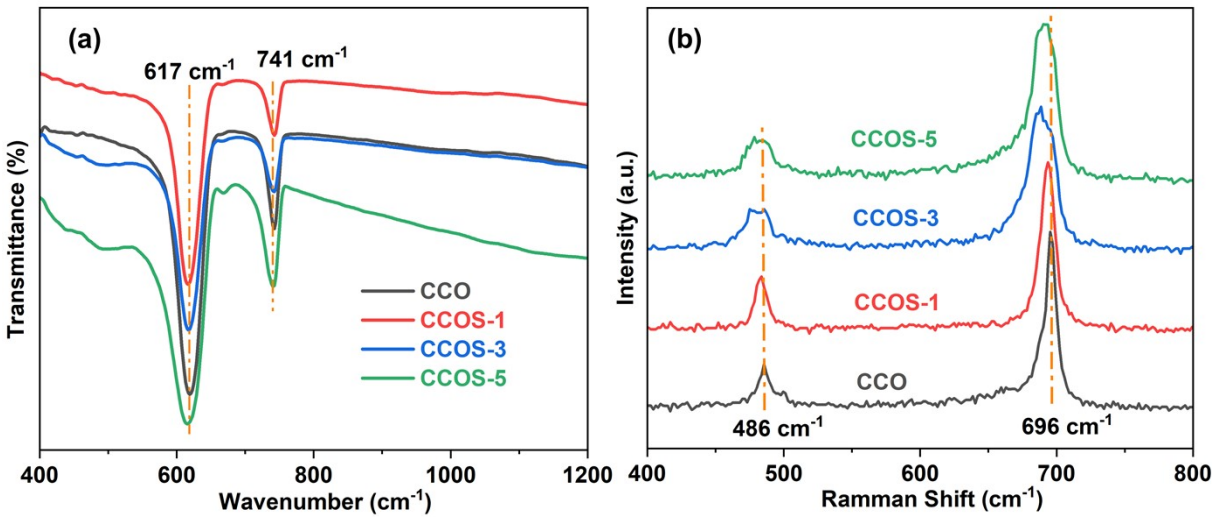

Fig. S6 Fourier transform infrared spectra (a) and Raman spectra (a) of CCO and CCOS-x s(x=1, 3 and 5).

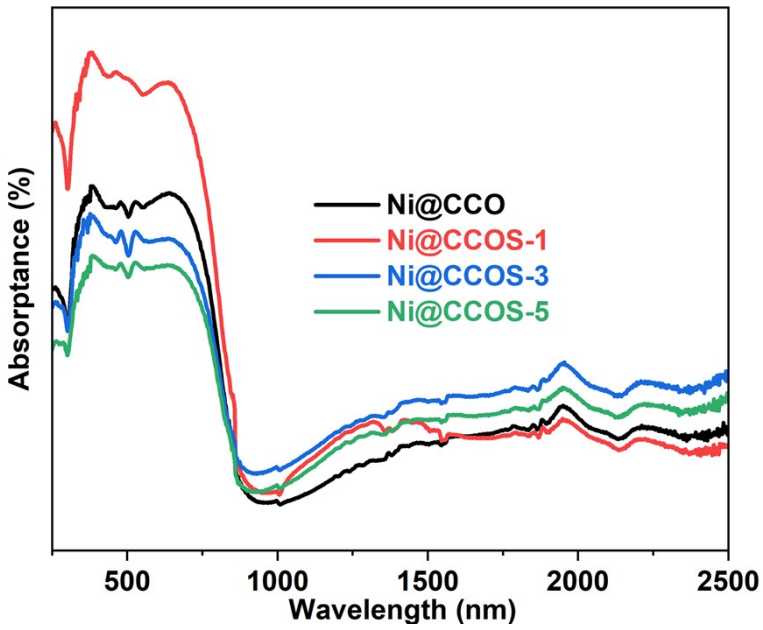

Fig. S7 UV-Vis-NIR absorption spectra CCO and CCOS-x (x=1, 3, 5).

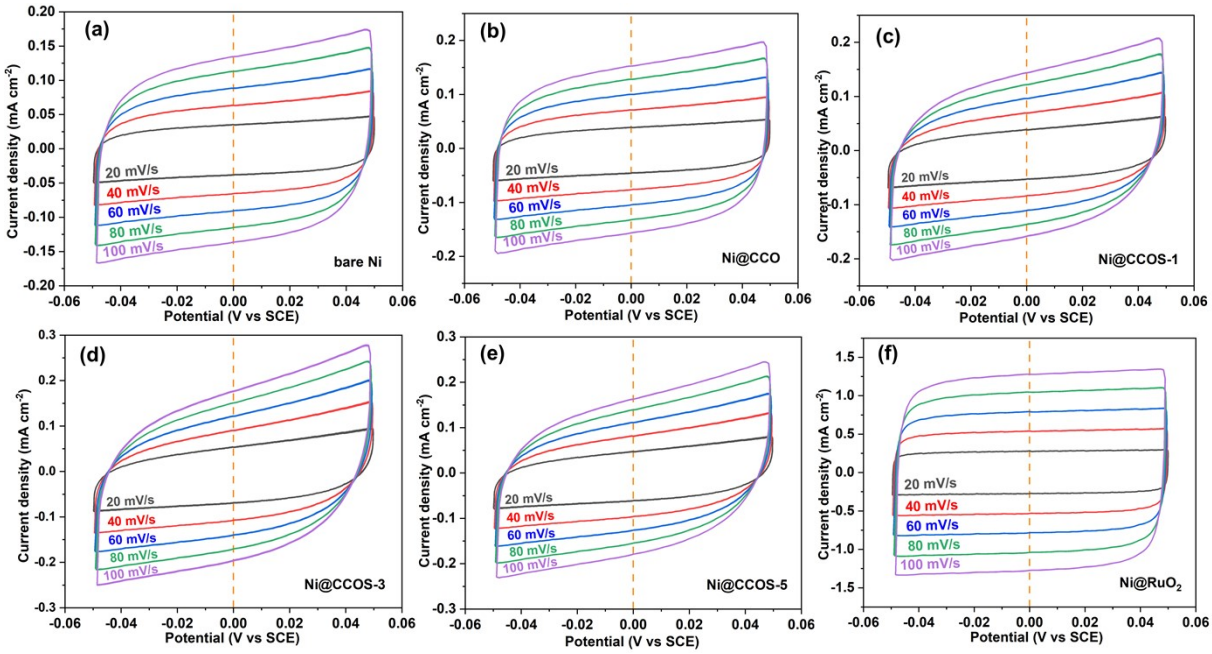

Fig. S8 CV curves of bare Ni (a), Ni@CCO, Ni@CCOS-x (x=1, 3, 5) and Ni@RuO_2 at different sweep speeds (such as 20, 40, 60, 80 and 100 mV/s).

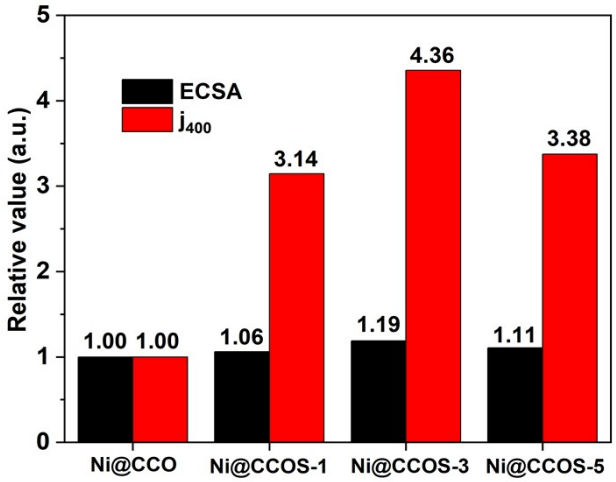

Fig S9 A summary of the key normalized parameters of Ni@CCO and Ni@CCOS-x (x=1, 3, 5) (ECSA; j_{400}: the current density at an overpotential of 400 mV).

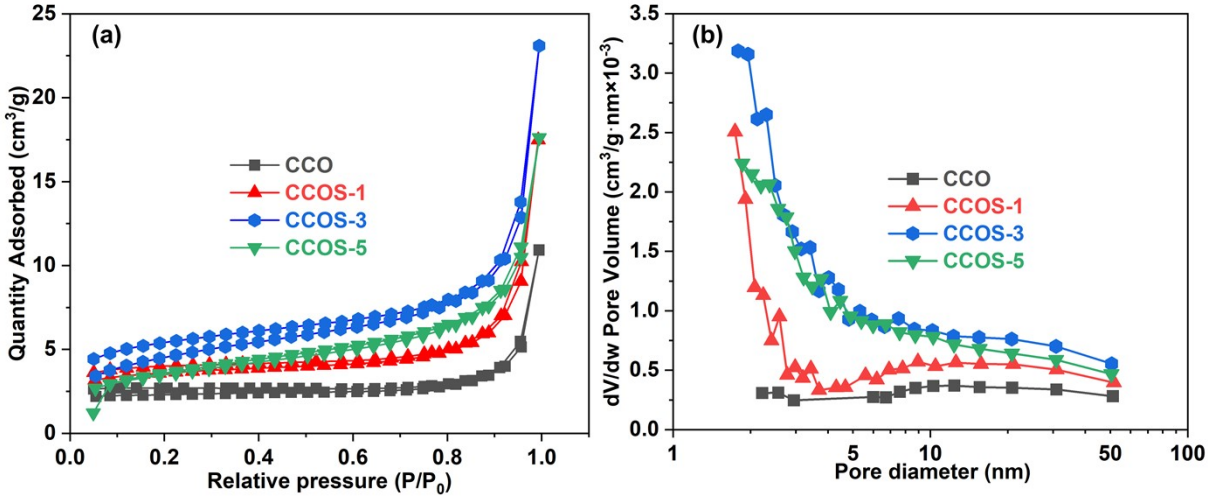

Fig. S10 N_2 adsorption-desorption isotherms (a) and pore structure (b) of CCO and CCOS-x (x=1, 3 and 5).

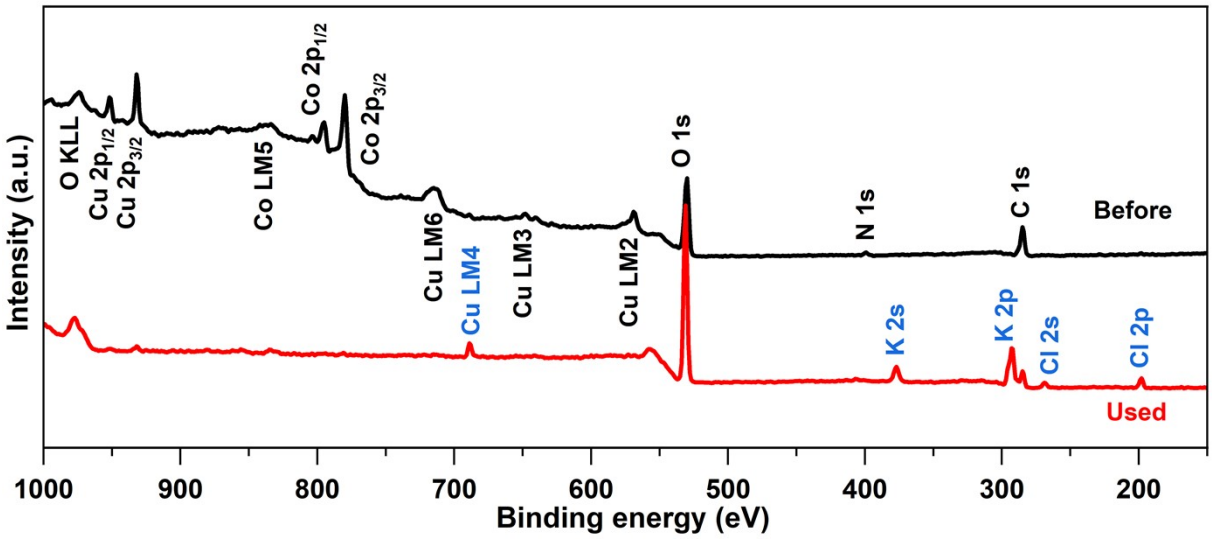

Fig. S11 The XPS survey spectra of CCOS-3 after an 18 hours continuous OER stability test.

References:

1 M. Yang, H. Tan, S. Ma*, et al.*, *Nanoscale*, 2023, **15**, 12375-12387.

2 S. Ma, J. Bai, L. Sun*, et al.*, *Dalton Transactions*, 2023, **52**, 13750-13757.

3 S. Ma, C. Jiang, J. Bai*, et al.*, *Inorganic Chemistry Frontiers*, 2024,**11**, 3482-3493.

4 H. Gao, M. Yang, X. Liu, et al., *Frontiers of Optoelectronics*, 2022, **15**, 8.

5 R. Chen, Z. Wang, S. Chen, et al., *ACS Energy Letters*, 2023, **8**, 3504-3511.

6 M. Ya, J. Wang, G. Li, et al., *ACS Sustainable Chemistry & Engineering*, 2023, **11**, 744-750.

7 J. Zhang, Y. Ye, B. Wei, et al., *Applied Catalysis B-Environment and Energy*, 2023, **330**, 122661.

8 J. J. Huang, T. Su, H. B. Zhao, et al., *Fuel*, 2024, **356**, 129479.

9 Z. Zhang, H. Sun, J. Li, et al., *Journal of Power Sources*, 2021, **491**, 229584.

10 M. W. Guo, Z. M. Wei and Q. B. Zhang, *International Journal of Hydrogen Energy*, 2022, **47**, 6029-6043.

11 N. A. Khan, I. Ahmad, N. Rashid, et al., *International Journal of Hydrogen Energy*, 2023, **48**, 31142-31151.

12 Z. Sun, C. Zhi, Y. Sun, et al., *Inorganic chemistry*, 2023, **62**, 21461-21469.

13 M. Kuang, P. Han, Q. Wang, et al., *Advanced Functional Materials*, 2016, **26**, 8555-8561.

14 A. Yadav, Y. Hunge, S. Kulkarni, et al., *Journal of colloid and interface science*, 2020, **576**, 476-485.

15 Q. Du, P. Su, Z. Cao, et al., *Sustainable Materials and Technologies*, 2021, **29**, e00293.